

Magnetic and electronic properties of bimagnetic materials comprising cobalt particles within hollow silica decorated with magnetite nanoparticles

T. Okada,^{1,a)} Y. González-Alfaro,^{2,3} A. Espinosa,^{2,b)} N. Watanabe,¹ T. Haeiwa,⁴ M. Sonehara,⁵ S. Mishima,¹ T. Sato,⁵ A. Muñoz-Noval,⁶ P. Aranda,² M. Garcia-Hernández,² and E. Ruiz-Hitzky^{2,a)}

¹Department of Chemistry and Material Engineering, Shinshu University, Wakasato 4-17-1, Nagano 380-8553, Japan

²Instituto de Ciencia de Materiales de Madrid (ICMM), CSIC, Cantoblanco, E-28049 Madrid, Spain

³Centro de Estudios Avanzados de Cuba (CEAC), CITMA, La Lisa, 17100 La Habana, Cuba

⁴Department of Computer Science, Shinshu University, Wakasato 4-17-1, Nagano 380-8553, Japan

⁵Department of Electrical and Electronic Engineering, Shinshu University, Wakasato 4-17-1, Nagano 380-8553, Japan

⁶SpLine Spanish CRG Beamline at ESRF, 6 Rue Jules Horowitz, BP 220, 38043 Grenoble Cedex 09, France

(Received 27 June 2013; accepted 18 August 2013; published online 24 September 2013)

Bimagnetic materials were fabricated by decorating the external surface of rattle-type hollow silica microspheres (which themselves contain metallic cobalt nanoparticles) with magnetite nanoparticles; thus, each magnetic substance was spatially isolated by the silica shell. The amount of magnetite decoration on the co-occluded hollow silica was varied from 1 to 17 mass %. Magnetic and electronic properties of the resulting bimagnetic materials were characterized by superconducting quantum interference device measurements and X-ray absorption spectroscopy, respectively. The ferrous iron in the bimagnetic sample was slightly more oxidized than in the magnetite reference, probably from some charge-transfer because of the SiO₂ surface contact, although the overall oxidation state of the samples is very similar to that of magnetite. The temperature dependence of the sample magnetization recorded with Zero Field Cooling and Field Cooling resulted in blocking temperatures for the bimagnetic materials that were close to that of magnetite nanoparticles (176 K) and were lower than that for the bare Co-occluded hollow silica (which was above room temperature). Values of coercive force and exchange bias at 300 K became quite small after decoration with only minimal amounts of magnetite nanoparticles (1–3 mass %) and were lower than those of magnetite. This is the first example of enhancing superparamagnetism by spatial separation of both Co and magnetite magnetic nanoparticles using a thin wall of diamagnetic silica. © 2013 AIP Publishing LLC. [<http://dx.doi.org/10.1063/1.4822299>]

I. INTRODUCTION

Soft magnetic materials, which exhibit high magnetic susceptibility and lower coercive forces at room temperature, have been investigated widely for applications in both chemical and biomedical fields for separation, transportation, sensing, and imaging using an external magnetic field.^{1–6} Among these materials, nano-sized magnetic particles have received much attention, but their tendency to aggregate often limits the practical use of magnetic nanoparticles (NPs). Agglomeration of the nanoparticles must be suppressed to maintain their nanomagnetic function; one way of doing this is to create core-shell or A@B particles (A: core, B: shell). These have been prepared through various synthetic strategies, including the use of self-assembled monolayers, layer-by-layer deposition, and sol-gel reactions.^{6–9} Recently, a new approach has been presented, where magnetite nanoparticles bonded to oleic acid molecules have been anchored to solid surfaces, and the final

materials exhibit superparamagnetism.¹⁰ This superparamagnetic nature is important for magnetic separations, as it allows easy recovery and dispersion in response to external magnetic fields.

High magnetic susceptibility is an inherent advantage of using pure metallic magnetic nanoparticles (e.g., Co, Fe, and Ni) as the core substances, especially for magnetically collectable catalysts, biomedical applications,^{11,12} and high-frequency applications, such as inductors,¹³ antennas, and noise suppressors.¹⁴ However, the pure core metals are prone to oxidation in air, and therefore, preventing this oxidation is a prerequisite to exploiting the improved magnetic properties (e.g., decreasing exchange bias). Attempts have been made to fabricate core-shell particles, where the shells can protect the pure metallic nanoparticle cores.^{15–21} We have recently reported synthesis of rattle-type Co@SiO₂ particles using a water-in-oil (W/O) emulsion system as template.²² Since these particles have dense silica shells, good stability of the inner Co particles has been shown when exposed to an acidic aqueous solution. However, partial oxidation of Co in air has been observed. In addition, the coercive force is still large because of the residual ferromagnetic (FM)

^{a)}Authors to whom correspondence should be addressed. Electronic addresses: tomohiko@shinshu-u.ac.jp and eduardo@icmm.csic.es

^{b)}Present address: Université Paris 7 Diderot, Paris, France.

characteristics of the metallic Co particles. Therefore, the performance as soft magnetic materials is insufficient for such applications.

Here, we propose a different approach to improve the performance, using magnetite nanoparticles to decorate the external surface of the Co@SiO₂ particles. Enhanced magnetic properties, which are neither achievable with any of the components alone nor by their physical mixture, have been shown to arise from *direct bonding* at the interfaces between two materials, exhibiting ferrimagnetic (FiM)-FM exchange coupling.²³ In the present system, each magnetic moiety has been *spatially isolated* by the silica shell. As a result, the coercive force and exchange bias were successfully decreased by decoration with only a small amount of magnetite (1–3 mass %). In addition, the final values of coercive force and exchange bias are lower than those of bare magnetite nanoparticles. The detailed results and a possible mechanism will be described in this paper.

II. EXPERIMENTAL

A. Materials

Octyltrichlorosilane (OTCS) and methyltrichlorosilane (MTCS) were purchased from Sigma-Aldrich Chemical Co., Ltd. (St. Louis, MO) and Shin-Etsu Chemical Co., Ltd. (Tokyo), respectively. Cobalt (II) nitrate hexahydrate and isooctane (2,2,4-trimethylpentane) were purchased from Wako Chemical Co., Ltd. (Osaka). These materials were used as received.

Oleic acid (99% purity), FeCl₃·6H₂O, FeSO₄·7H₂O (Sigma-Aldrich), ultra pure water (resistivity of 18.2 MΩ·cm), and aqueous ammonia solution (28% purity, Fluka) were used in the synthesis of the magnetic NPs.

B. Sample preparation

Rattle-type Co core and silica shell particles (Co@SiO₂) were prepared based on a previously reported procedure.²² A W/O emulsion was prepared by mixing 0.22 ml of water, 0.75 ml of Co(NO₃)₂ aqueous solution (3.0 mol kg⁻¹), and 2.97 g of OTCS in 50 ml of isooctane under ultrasonic agitation. After 5 min of ultrasonic irradiation (45 kHz, 100 W), the mixture was allowed to stand for 5 min at room temperature. The ultrasonic agitation was repeated three times. Then 1.34 g of MTCS in 10 ml of isooctane was poured into the W/O emulsion under magnetic stirring. The mixture was stirred at room temperature for more than 3 h to make polymethylsiloxane shells around aqueous droplets. During the reaction, air saturated with water vapor (ca. 0.1 l min⁻¹) was continuously supplied. The resulting solid obtained was separated by filtration, followed by washing thoroughly with isooctane and drying at 323 K for 1 day.

The dried product was heated at 393 K in air for 1 day, and then calcined at 873 K in an electronic furnace for 3 h. The calcined product was treated under H₂ flow (5 ml min⁻¹) at 773 K for 3 h, and subsequently heated at 973 K for 3 h in N₂ flow (10 ml min⁻¹). The resulting product was then washed with 1 mol l⁻¹ HCl. The acid-treated sample was recovered using neodymium magnets, whose surface magnetic

field is 3.8 kOe, located at both sides of a glass bottle (outer diameter of 26 mm). The magnetic field gradient from the center of the glass bottle to the magnet was 150 kOe·m⁻¹. The recovered sample was thoroughly washed with water before further magnetic recovery.

Oleic acid-magnetite NPs were prepared by an approach based on that previously described.²⁴ A ferrofluid was prepared using *n*-heptane (10 ml) and further assembled onto the Co@SiO₂ sample as reported in Refs. 10 and 25. Bimagnetic materials consisting of Co@SiO₂ externally decorated with the NPs were prepared by mixing both systems to reach ca. 50 mg of solids with final oleic acid-magnetite/Co@SiO₂ mass ratios as listed in Table I. Finally, the solvent was removed by evaporation at room temperature, recovering a gray solid, the darkness of the gray depended on the magnetite NP content.

C. Materials characterization

X-ray powder diffraction (XRD) patterns were obtained by using a Rigaku RINT 2200V/PC diffractometer (monochromatic Cu Kα radiation), operated at 20 mA, 40 kV. Scanning electron micrographs (SEM) were obtained on a Hitachi S-4100 field-emission scanning electron microscope (accelerating voltage 15 kV). Scanning transmission electron micrographs (STEMs) were obtained on a Hitachi High-Tech HD-2300A spherical aberration corrected scanning transmission electron microscope (acceleration voltage of 200 kV). Inductively coupled plasma atomic emission spectroscopy (ICP-AES) was performed on a Shimadzu ICPS-7500.

D. Magnetic characterization

The magnetic characterization of the samples at low and high temperatures (5 and 300 K) was carried out using a Superconducting Quantum Interference Device (SQUID) from Quantum Design. Magnetization curves at 5 K and the temperature dependence of the magnetization of samples were recorded upon Zero Field Cooling (ZFC) and Field Cooling (FC) protocols with H_{FC} = 1 T and a measuring field of 50 Oe.

E. Electronic properties (X-ray absorption spectroscopy, XAS)

XAS measurements at the Fe K-edge (E = 7110 eV) in the near edge regime (XANES) spectroscopy were performed

TABLE I. List of sample numbers and compositions.

#Sample	Oleic acid-magnetite NPs (%)	Co@SiO ₂ (%)
1	1.2	98.8
2	3.0	97.0
3	5.7	94.3
4	11.4	88.6
5	16.6	83.4
6	0	100
7	100	0

on the Spanish beamline (SpLine) at the European Synchrotron Radiation Facilities (ESRF) located in Grenoble, France. The spectra were obtained in fluorescence detection mode. The powder samples were deposited onto silicon substrates and held with Kapton tape. Data analysis was carried out using the “Athena”²⁶ program.

III. RESULTS AND DISCUSSION

A. Decoration of Co@SiO₂ with magnetite nanoparticles

1. Preparation of Co@SiO₂

A SEM image of the Co@SiO₂ particles is shown in Figure 1(a). The average particle size of the particles was estimated as 0.3 μm ($N = 1.3 \times 10^3$). A rattle-type core-shell structure was observed in the bright-field TEM image

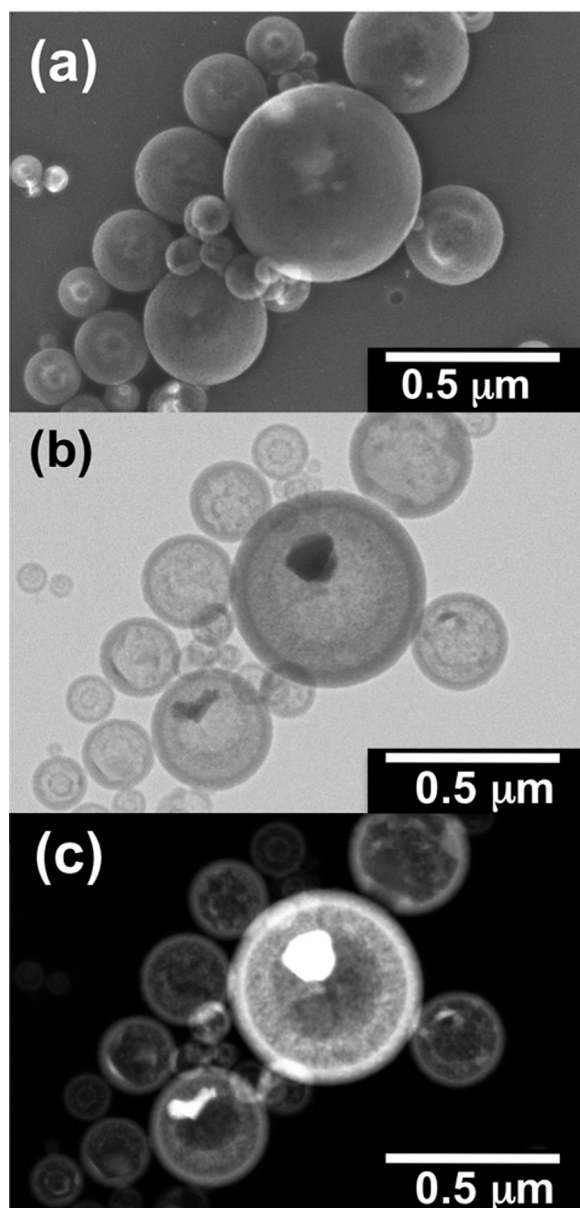


FIG. 1. (a) SEM image, (b) bright-field TEM image, and (c) STEM dark-field image of the Co@SiO₂ sample.

(Figure 1(b)). The STEM dark-field image (Figure 1(c)) indicated that the majority of Co is within the void spaces of the spherical hollow silica particles. ICP analysis showed that the amount of Co in the Co@SiO₂ was 7 mass %. XRD analysis revealed that CoO co-exists with metallic Co in Co@SiO₂.

2. Decoration of Co@SiO₂ with magnetite NP

SEM and TEM images of three selected samples of the magnetite NP decorated Co@SiO₂ (samples #1, #3 and #5, containing 1.2, 5.7, and 16.6 mass % of oleic acid-magnetite NPs, respectively) are shown in Figure 2. Magnetite NPs were observed on the surface of the Co@SiO₂ particles. The particle size of the NPs estimated from the TEM images was less than 20 nm, which was close to the size of the bare oleic acid-magnetite NPs.¹⁰ When the amount of NPs is smaller (ca. 1.2 and 5.7 mass % in Figs. 2(a) and 2(b), respectively), the magnetite NPs appear homogeneously distributed on the external surface of the Co@SiO₂ particles. In contrast, the magnetite NPs tend to agglomerate on the Co@SiO₂ surface when the NP content is higher, i.e., for the sample containing ca. 17 mass %, as shown in Figure 2(c).

B. Magnetic properties

Figures 3(a) and 3(b) show the magnetization curves of the Co@SiO₂ sample without magnetite NPs and of the NPs, respectively, at temperatures of 5 and 300 K. Since both curves exhibit hysteresis loops, both samples show ferromagnetic properties; however, their magnetic behavior is quite different, and values of saturation magnetization (M_s), coercive fields (H_c), blocking temperature (T_B), irreversibility temperature (T_{irr}), and exchange bias (H_{EB}) are presented in Table II. While the Co@SiO₂ sample is characterized by a higher coercivity, a non-saturated signal is observed at low temperature (5 K), possibly because of the presence of paramagnetic and/or antiferromagnetic phases. On the other hand, the NPs are nearly in their superparamagnetic regime at 300 K, showing larger M_s values close to that of bulk magnetite ($\sim 80 \text{ emu/g}$).²⁷ Moreover, the sharpest loops are observed for the NPs, indicating rapid rotation of the magnetization of the magnetic nanoparticles with increasing field.

The ZFC/FC hysteresis loops at low temperature are shifted in the Co@SiO₂ sample, revealing an exchange bias (EB)²⁸ phenomenon ($\sim 30 \text{ Oe}$) related to the antiferromagnetic or ferrimagnetic phases that could lead to pinning effects in the ferromagnetic domains. This is probably due to a thin shell of CoO. This effect is hardly detected in the bare NPs.

Low field ZFC-FC magnetization curves of these references are shown in Figure 4. The NP curves exhibit the typical blocking process of an assembly of superparamagnetic particles with a distribution of blocking temperatures, as seen in Figure 4(b), and the overall T_B is around 175 K. In contrast, the Co@SiO₂ sample presents a wider distribution of magnetic domain sizes and shows a blocking temperature well above 400 K (Figure 4(a)). Moreover, an increase in the

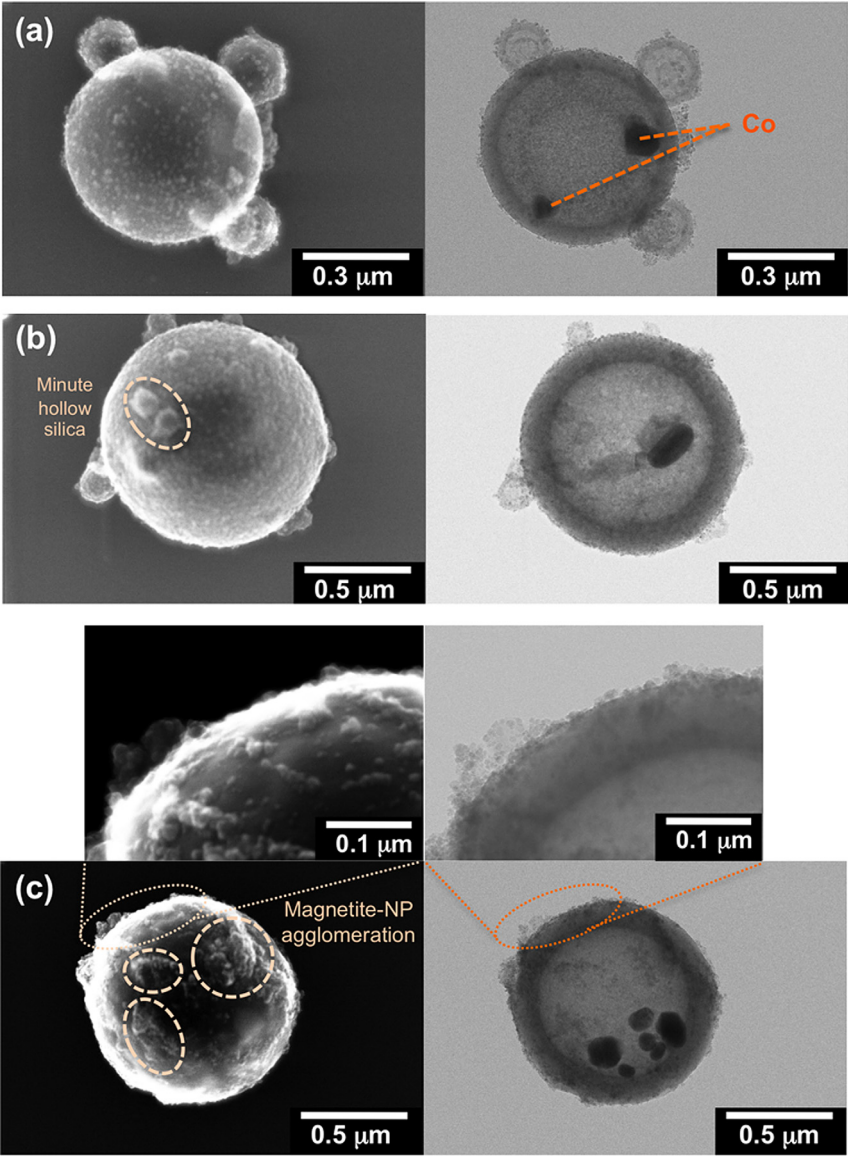


FIG. 2. SEM (left side) and TEM (right side) images of the representative Co@SiO₂ samples decorated with magnetite NPs. Parts (a)–(c) correspond that the amounts of NP on Co@SiO₂ are 1.2, 5.7, and 16.6 mass % (sample #1, #3, and #5), respectively.

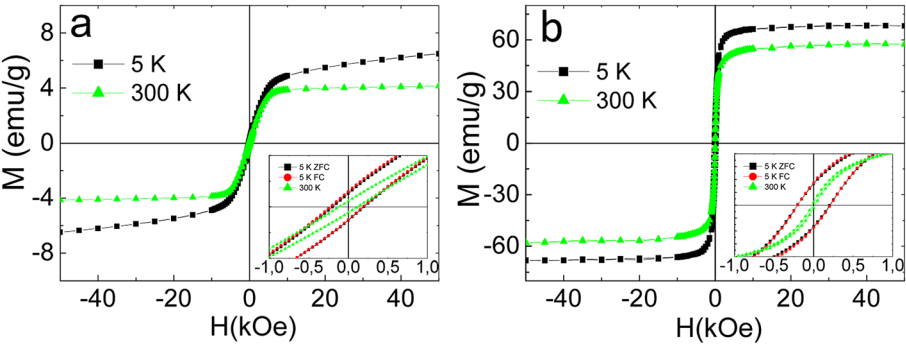


FIG. 3. Field-dependent magnetization curves at 5 K and 300 K of the (a) Co@SiO₂ sample (sample #6) without decorated NPs and (b) of magnetite NPs (sample #7). Inset: detail of the low field region of hysteresis loops at 300 K and 5 K under ZFC and FC conditions (H_{FC} = 10 kOe).

TABLE II. Magnetic properties of the samples.

Sample#	Magnetite NP (%)	Co@SiO ₂ (%)	<i>M</i> _s (300 K) (emu g ⁻¹)	<i>T</i> _B (K)	<i>T</i> _{irr} (K)	<i>H</i> _c (5 K) (Oe)	<i>H</i> _c (300 K) (Oe)	<i>H</i> _{EB} (Oe)
1	1.2	98.8	5.44	153	425	341	6	5.5
2	3.0	97.0	5.35	153	425	326	6	3.0
3	5.7	94.3	7.35	159	400	336	10	1.0
4	11.4	88.6	10.2	172	350	330	13	1.0
5	16.6	83.4	12.9	172	300	330	16	0.5
6	0	100	3.98	350	~500	201	117	29
7	100	0	56.2	176	348	214	21	2.0

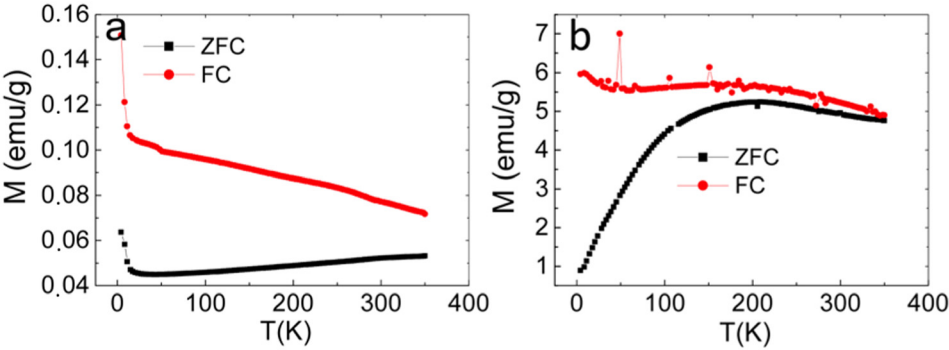


FIG. 4. Low field ZFC-FC magnetization of the (a) Co@SiO₂ (sample #6) and (b) of the magnetite NPs (sample #7).

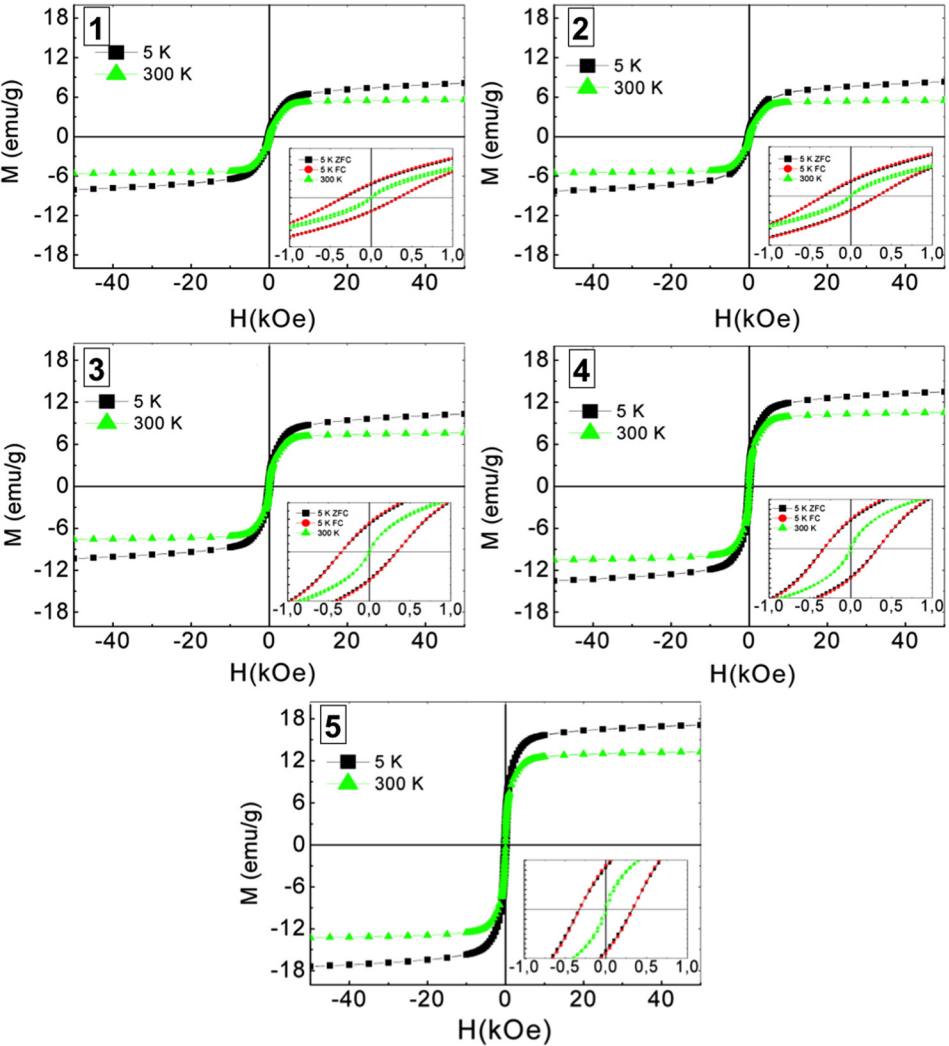


FIG. 5. Field-dependent magnetization curves at 5 K and 300 K of the different samples (#1 to #5) as the percent increases: the percentages of NPs are (1) 1.2, (2) 3.0, (3) 5.7, (4) 11.4, and (5) 16.6 mass %. Inset: detail of the low field region of hysteresis loops at 300 K and 5 K under ZFC and FC conditions ($H_{FC} = 10$ kOe).

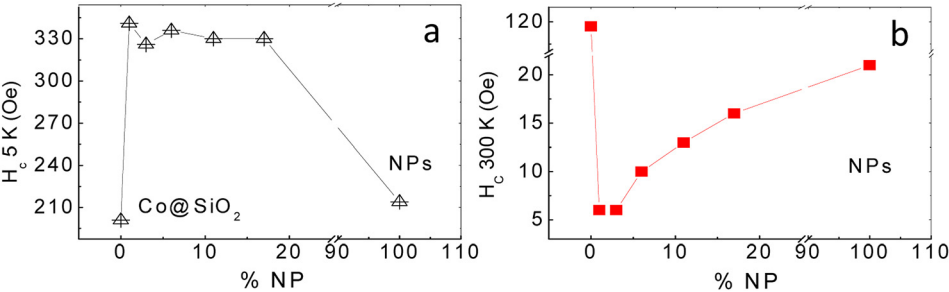
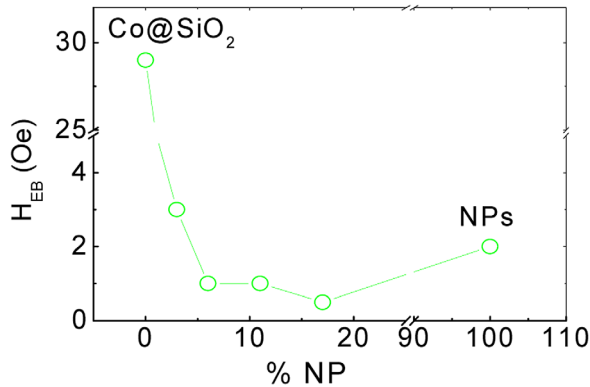


FIG. 6. Coercive fields H_c at (a) 5 K and at (b) 300 K.

FIG. 7. Exchange bias H_{EB} values of the samples.

magnetic signal at lower temperatures indicates a paramagnetic contribution in both ZFC and FC curves for the Co@SiO₂ sample.

Magnetization curves at 300 K and 5 K (ZFC/FC protocols) of Co@SiO₂ decorated with various amounts of magnetite NPs are displayed in Figure 5. As the percentage of magnetite NPs increases, the curves saturate at higher M_s values and the non-saturated signal at 5 K loses prominence. The M_s values of the different samples are listed in Table II.

Normalization of the magnetization data was done in relation to the total mass of each sample in order to avoid a priori assumptions on the NPs growth and distribution and its possible effect on surface magnetism as well as on the presence of magnetic frustration in the system. As the NP content increases, the magnetic properties evolve to be closer to those of the bare NPs, showing a combination of both NP and Co behaviors in magnetization.

The coercivity value (H_c) at 5 K is greater for the Co@SiO₂ sample decorated with magnetite NPs than for either of the component materials (Figure 6(a)). This behavior can be attributed to the existence of magnetic disorder at the interfaces of the NPs with the SiO₂ sphere; this disorder does not occur when the system contains only NPs. It is worth noting that there is no clear trend with the percent of NPs.

Interestingly, the H_c values at 300 K (Figure 6(b)) become extremely low for the Co@SiO₂ sample decorated with magnetite NPs, showing that superparamagnetism appeared at this temperature when the Co@SiO₂ sample was combined with magnetite NPs. The minimum value of H_c appears to be around 1–3 mass % NPs. This means that the magnetic anisotropy is greatly decreased near room temperature as a result of the decoration. As shown in Figure 7, the exchange bias (H_{EB}) value of the Co@SiO₂ sample (29 Oe)

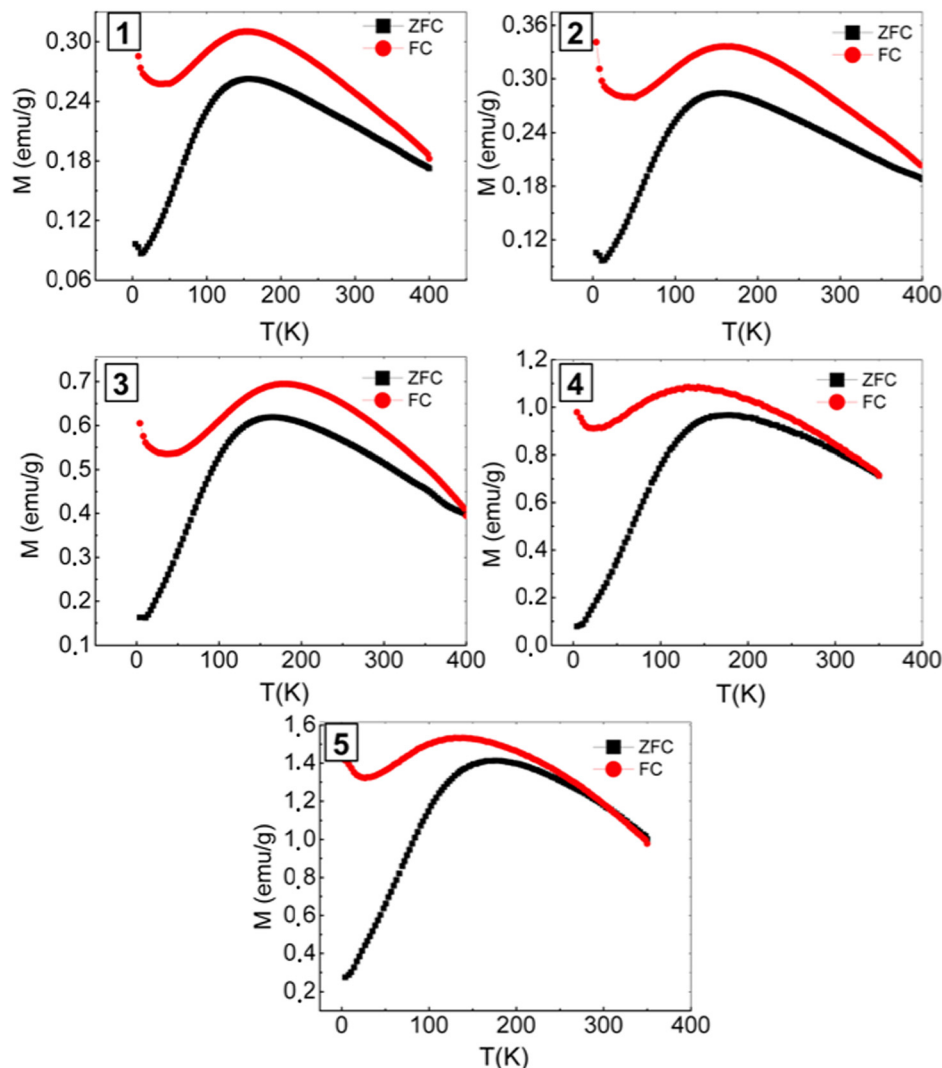


FIG. 8. Low field ZFC-FC magnetization of the different samples as the percent of NPs increases: the percentages are (1) 1.2, (2) 3.0, (3) 5.7, (4) 11.4, and (5) 16.6 mass %.

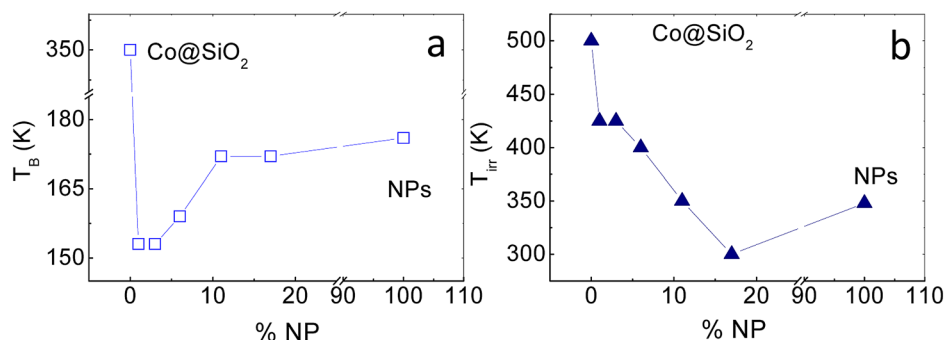


FIG. 9. (a) Blocking temperature (T_B) and (b) irreversibility temperature (T_{irr}) of the samples.

is significantly decreased by the decoration, presenting very low values (even lower than the 2 Oe for the bare NPs) as the NP content is increased (3%–17%). Since CoO still surrounds the Co in the void space of the SiO₂ hollow sphere, its contribution must be masked in some way by the behavior of the NPs.

Low-field ZFC/FC magnetization curves of Co@SiO₂ samples decorated with different amounts of magnetite NPs are shown in Figure 8. The temperature-dependent ZFC/FC curves show similar shapes to the curve for bare NPs (Figure 4(b)). The variation in the blocking temperatures (T_B) estimated from the curves as a function of the amounts of magnetite NPs in the samples is shown in Figure 9(a). The T_B values of the decorated samples (#1 to #5) were lower than those of the bare NPs. T_B increases with increasing NP content; this is consistent with aggregation of NPs at higher contents. As seen in the STEM images (Figure 2), agglomeration of the magnetite NPs occurred on the Co@SiO₂ surface at the highest loading of NPs (ca. 17 mass %), but was not seen at NP contents of 1–6 mass %.

The irreversibility temperature (T_{irr}), defined as the value where the ZFC and FC curves separate, is a way of comparing the two different magnetic behaviors to see how field cooling restricts the system. Movement of T_{irr} to lower values is observed as the NP content of the system increases, which leads to lower convergence of the curves (Figure 9(b)). Although the system is increasingly dominated by the

behavior of the iron oxide nanoparticles, the T_{irr} corresponding to bare NPs is higher than that of sample 5.

C. Electronic properties (XAS)

The normalized Fe K-edge absorption spectra of bare NPs and of decorated samples (1 and 5) are presented in Figure 10. The line shapes in samples 1 and 5 are very similar exhibiting the same transitions (peaks) as the spectrum of bare NPs, which is less intense possibly due to self-absorption effect. Oxidation state varies linearly with the energy edge position^{29,30} and in this case, samples 1 and 5 show similar valence state although they show differences in their magnetic behavior. Moreover, a slight shift in the energy edge has been observed in comparison with that of bare NPs, which exhibit an overall valence state similar to magnetite. Measuring magnetite and maghemite references in the same configuration as samples (fluorescence or transmission) could discriminate between magnetite and maghemite.³¹ Self-absorption effects in XANES spectra collected in the fluorescence mode induce modifications in the spectral shape of the compound that can lead to a misanalysis of the results. In this case, the fit must be done using the references also measured in the fluorescence mode and under the same experimental conditions to obtain a proper result. For this reason, we cannot rule out the presence of a fraction of maghemite in all the samples. On the other hand, the shift in the decorated samples (1 and 5) in comparison with bare nanoparticles can be ascribed to a charge-transfer process with the SiO₂ surface contact leading to an overall oxidation of Fe. Charge transfer processes are not unusual at interfaces involving iron oxides. Even direct observation of spin polarization conservation in charge transfer processes across colloidal magneto-plasmonic has been recently reported to occur in Au@Fe-oxide core@shell nanocrystal heterostructures.³²

IV. CONCLUSIONS

Micro-spherical hollow silica particles enclosing metallic cobalt partially oxidized to antiferromagnetic cobalt oxide nanoparticles (Co@SiO₂) were decorated with superparamagnetic magnetite NPs through treatment with ferrofluids. The decoration was conducted by preparing rattle-type Co-silica core-shell particles, followed by assembling oleic acid-magnetite dispersed in *n*-heptane.

XAS results on the bimagnetic materials indicated that the magnetite NPs were assembled on the external surface of the hollow particles and that a charge-transfer had occurred

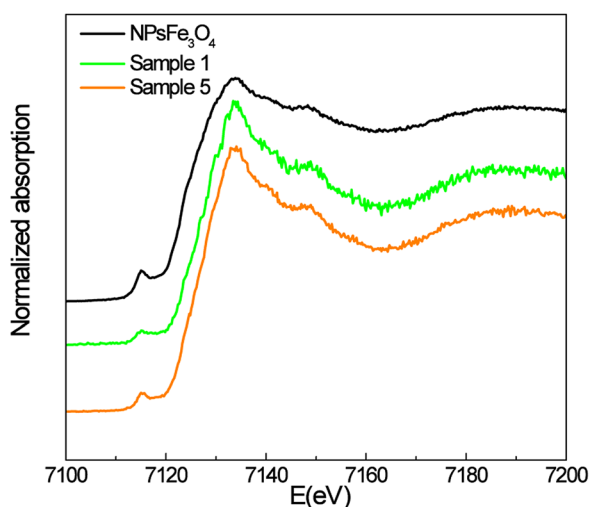


FIG. 10. Normalized Fe K-edge XANES spectra of the NPs decorated samples of #1 and #5 with 1.2 and 16.6 mass % NPs, respectively, together with that of the bare NPs (Fe₃O₄).

between ferrous iron and silica. However, the presence of maghemite cannot be ruled out from our fluorescence detection mode XANES experiments. Temperature-dependent magnetization after ZFC and ZC with an applied field H_{fc} of 1 T showed that the blocking temperatures for the bimagnetic materials (153–172 K) were close to that of the magnetite nanoparticles (176 K), irrespective of the amount of magnetite NP decoration. Although the values of coercive force at 5 K for the bimagnetic materials were higher than those of both undecorated core-shell particles and magnetite NPs, the coercive force at 300 K decreased to 6 Oe, much lower than that of magnetite NPs (21 Oe) even when the amount of magnetite NP decoration was small (1–3 mass %). In addition, the values of exchange bias were made negligible by the decoration. A possible explanation of this unusual superparamagnetism is that the spatial distribution, in which both types of magnetic nanoparticles (cobalt and magnetite NPs) are separated by the thin silica wall, causes magnetic disorder at the interfaces of the NPs with the silica spheres.

ACKNOWLEDGMENTS

T.O. thanks JSPS (Grant-in-Aid for Scientific Research, No. 23655143), JST (A-STEP), Nippon Sheet Glass Foundation for Materials Science and Engineering, and Shinshu University (Funding Program for Green Innovation) for financial support. Y.G.-A., P.A., and E.R.-H. thank CICYT (Spain, Project No. MAT2012-31759) for financial support. M.G.-H. and A.E. received financial support from MINECO Project No. MAT 2011 27470 and Consolider Ingenio CSD2009-00013. We acknowledge ESRF for beamtime and BM25 personnel for technical support.

¹V. Sokolova and M. Epple, *Angew. Chem., Int. Ed.* **47**, 1382 (2008).

²A. H. Latham and M. E. Williams, *Acc. Chem. Res.* **41**, 411 (2008).

³Y. W. Jun, J. W. Seo, and A. Cheon, *Acc. Chem. Res.* **41**, 179 (2008).

⁴U. Jeong, X. Teng, X. Y. Wang, H. Yang, and Y. Xia, *Adv. Mater.* **19**, 33 (2007).

⁵M. Mahmoudi, S. Sant, B. Wang, S. Laurent, and T. Sen, *Adv. Drug Delivery Rev.* **63**, 24 (2011).

⁶A.-H. Lu, E. L. Salabas, and F. Schüth, *Angew. Chem., Int. Ed.* **46**, 1222 (2007).

⁷F. Caruso, *Adv. Mater.* **13**, 11 (2011).

⁸X. W. Lou, L. A. Archer, and Z. Yang, *Adv. Mater.* **20**, 3987 (2008).

⁹V. Salgueiriño-Maceira and M. A. Correa-Duarte, *J. Mater. Chem.* **16**, 3593 (2006).

¹⁰Y. González-Alfaro, P. Aranda, F. M. Fernandes, B. Wicklein, M. Darder, and E. Ruiz-Hitzky, *Adv. Mater.* **23**, 5224 (2011).

¹¹D. L. Huber, *Small* **1**, 482 (2005).

¹²T.-Y. Liu, S.-H. Hu, D.-M. Liu, S.-Y. Chen, and I.-W. Chen, *Nano Today* **4**, 52 (2009).

¹³H. Ito, A. Takeuchi, S. Okazaki, H. Kobayashi, Y. Sugawa, A. Takeshima, M. Sonehara, N. Matsushita, and T. Sato, *IEEE Trans. Magn.* **47**, 3204 (2011).

¹⁴M. Sonehara, T. Sato, K. Yamasawa, and Y. Miura, *J. Magn. Soc. Jpn.* **33**, 293 (2009).

¹⁵Y. Kobayashi, M. Horie, M. Konno, B. Rodríguez-González and L. M. Liz-Marzán, *J. Phys. Chem. B* **107**, 7420 (2003).

¹⁶Y. Leng, K. Sato, Y. Shi, J.-G. Li, T. Ishigaki, T. Yoshida, and H. Kamiya, *J. Phys. Chem. C* **113**, 16681 (2009).

¹⁷Y. D. Liu, H. J. Choi, and S.-B. Choi, *Colloid Surf., A* **403**, 133 (2012).

¹⁸A. H. Lu, W. C. Li, N. Matoussevitch, B. Spliethoff, H. Bonnemann, and F. Schüth, *Chem. Commun.* **2005**, 98.

¹⁹A.-H. Lu, W. Schmidt, N. Matoussevitch, H. Bonnemann, B. Spliethoff, B. Tesche, E. Bill, W. Kiefer, and F. Schüth, *Angew. Chem., Int. Ed.* **43**, 4303 (2004).

²⁰I.-S. Park, M. Choi, T.-W. Kim, and R. Ryoo, *J. Mater. Chem.* **16**, 3409 (2006).

²¹M. Aslam, S. Li, and V. P. Dravid, *J. Am. Ceram. Soc.* **90**, 950 (2007).

²²T. Okada, N. Watanabe, T. Haeiwa, T. Sakai, and S. Mishima, *Chem. Lett.* **40**, 106 (2011).

²³M. Casavola, A. Falqui, M. A. García, M. García-Hernández, C. Giannini, R. Cingolani, and P. D. Cozzoli, *Nano Lett.* **9**, 366 (2009).

²⁴W. Zhang, F. Gao, and H. Gu, *J. Magn. Magn. Mater.* **288**, 403 (2005).

²⁵E. Ruiz-Hitzky, P. Aranda, and Y. González-Alfaro, Spanish patent 201030333 (2010); PCT ES2011/070145 (2011).

²⁶M. Newville, *J. Synchrotron Rad.* **8**, 322 (2001).

²⁷B. D. Culliti and C. D. Graham, *Introduction to Magnetic Materials* (John Wiley & Sons, New Jersey, 2009).

²⁸J. Nogués and I. K. Schuller, *J. Magn. Magn. Mater.* **192**, 203 (1999).

²⁹V. Kunzl, *Collect. Trav. Chim. Tchecolovaquie* **4**, 213 (1932).

³⁰A. Corrias, G. Mountjoy, D. Loche, V. Puentes, A. Falqui, M. Zanella, W. J. Parak, and M. F. Casula, *J. Phys. Chem. C* **113**, 18667 (2009).

³¹A. Espinosa, A. Serrano, A. Llavona, J. Jimenez de la Morena, M. Abuin, A. Figuerola, T. Pellegrino, J. F. Fernández, M. Garcia-Hernandez, G. R. Castro, and M. A. Garcia, *Meas. Sci. Technol.* **23**, 015602 (2012).

³²F. Pineider, C. de Julián Fernández, V. Videtta, E. Carlino, A. al Hourani, F. Wilhelm, A. Rogalev, P. D. Cozzoli, P. Ghigna, and C. Sangregorio, *ACS Nano* **7**, 857 (2013).